The effect of ion orbit loss and X-loss on the interpretation of ion energy and particle transport in the DIII-D edge plasma

Weston M. Stacey
Fusion Research Center, Georgia Institute of Technology, Atlanta, Georgia 30332, USA

(Received 30 June 2011; accepted 18 August 2011; published online 14 October 2011)

Calculation models are presented for treating ion orbit loss effects in interpretive fluid transport calculations for the tokamak edge pedestal. Both standard ion orbit loss of particles following trapped or passing orbits across the separatrix and the X-loss of particles that are poloidally trapped in a narrow null-B_θ region extending inward from the X-point, where they gradB and curvature drift outward, are considered. Calculations are presented for a representative DIII-D [J. Luxon, Nucl. Fusion **42**, 614 (2002)] shot which indicate that ion orbit loss effects are significant and should be taken into account in calculations of present and future experiments. © *2011 American Institute of Physics*. [doi:10.1063/1.3640506]

I. INTRODUCTION

It has long been recognized that an understanding of the physics of the tokamak edge plasma was important to achieving an understanding of tokamak performance, and tokamak edge pedestal physics has long been (e.g., Ref. 1) and remains (e.g., Ref. 2) an active area of tokamak physics research. A relationship between changes in the radial electric field E_r and in the poloidal rotation velocity V_θ in the plasma edge and changes in the edge pressure, temperature, and density gradients in the plasma edge has long been observed experimentally,[3] suggesting that an understanding of the causes of the rotation velocities and the radial electric field may provide insight to an understanding of edge pedestal physics, and recently it has been demonstrated that changes in these experimentally observed quantities are correlated by momentum balance requirements.[4–6] A second, and more widely held, school of thought postulates that the stabilization or destabilization of electromagnetic microinstabilities[7–9] and the corresponding changes in fluctuation-driven transport cause the observed changes in temperature and density gradients in order for diffusive heat and particle fluxes to remove the input heat and particles. A third school of thought is that the physics of the edge plasma is determined, at least in part, by the loss of energetic ions and their consequences.[10–23] Finally, the ionization of recycling neutral atoms[24,25] and magneto-hydrodynamic (MHD) instabilities[26] also have been suggested as causes of the observed edge pedestal structure.

The reason that it is important to understand the pedestal physics and to develop a predictive capability for the edge pedestal is that it seems to determine the performance of future tokamaks,[27,28] such as ITER. For this reason, there are a large number of people worldwide trying to understand edge pedestal physics. Most of these people are working with 1D or 2D transport codes which model the edge pedestal and sometimes the scrape-off layer in fluid theory, but usually without taking ion orbit loss effects into account. For example, the National H-Mode Edge Pedestal (HEP) Group[29] are interpreting DIII-D edge data with 1D codes such as ONE-TWO[30] and GTEDGE,[31] and with 2D codes such as UEDGE[32] and SOLPS.[33] One of the major objectives of this HEP and similar work is to determine particle and energy fluxes that can be used to interpret the measured density and temperatures in order to infer the experimental values of heat and particle diffusivities in the edge pedestal for comparison with theoretical transport models (e.g., Refs. 29 and 34). Ion orbit loss effects presently are not taken into account in this and similar interpretations of experimental data, nor in other work using the same and similar codes to calculate heat load distributions on the chamber wall and into the divertor.

Ion orbit loss effects could significantly alter the results of most of the ongoing work on edge plasma physics experimental interpretation and prediction. Thus, the primary purposes of the work reported in this paper are (i) to develop computationally tractable models that can be used to take into account the effect of ion orbit losses on the interpretations and predictions of experimental data made with fluid codes and (ii) to investigate the magnitude of ion orbit loss effects on the interpretation of ion thermal diffusivities in DIII-D.[35]

There are two different basic mechanisms for ion orbit loss in the edge plasma. The most familiar is the case of ions on passing or banana-trapped orbits that leave the plasma by drifting outward across the last closed flux surface (e.g., Refs. 11, 36, and 37). Both thermalized plasma ions and energetic neutral beam ions (and fusion alpha particles) can be lost in this manner. This type of ion orbit loss will be referred to as "standard" ion orbit loss.

A second ion orbit loss mechanism, more recently elaborated by C. S. Chang and colleagues,[18–25] is an ion loss through the X-point in diverted plasmas associated with the fact that ions on orbits that pass near the X-point where the poloidal magnetic field is very small have a very small poloidal displacement in time and are essentially trapped in the poloidal vicinity of the X-point, where they are subject to vertical curvature and grad-B drifts which take them outward across the last closed flux surface and eventually into the divertor. The poloidal motion of the electrons is sufficient that they are not affected by this trapping mechanism, so there is effectively a radially outward ion current which builds up an inward-directed radial electric field. This radial electric field

interacts with the toroidal magnetic field to produce an *ExB* poloidal drift that de-traps the ions by allowing them to drift poloidally to field lines that are not trapped in the vicinity of the X-point. Thus, the ion orbit loss rate is determined by the relative values of the vertical curvature and grad-B drift loss rate and of the de-trapping *ExB* poloidal drift rate. The work to date[18–23] on this "X-loss" ion orbit loss largely has made use of computationally intensive particle orbit calculations, which are impractical for routine analysis in conjunction with edge fluid code analyses such as those used by the members of the HEP group. This type of ion orbit loss will be referred to as "X-loss".

II. MODELING OF STANDARD ION ORBIT LOSS

Following Miyamoto[11] and others, we make use of the conservation of canonical toroidal angular momentum,

$$RmV_{\|}f_{\varphi} + e\psi = const = R_0 m V_{\|0} f_{\varphi 0} + e\psi_0, \tag{1}$$

to write the orbit constraint for an ion introduced at a location "0" on flux surface ψ_0 with parallel velocity $V_{\|0}$, where $f_{\varphi} = |B_{\varphi}/B|$, R is the major radius, and ψ is the flux surface value. The conservation of energy and of poloidal angular momentum,

$$\begin{aligned} &\frac{1}{2}m(V_{\|}^2 + V_{\perp}^2) + e\phi = const = \frac{1}{2}m(V_{\|0}^2 + V_{\perp 0}^2) \\ &\quad + e\phi_0 \equiv \frac{1}{2}mV_0^2 + e\phi_0, \\ &\frac{mV_{\perp}^2}{2B} = const = \frac{mV_{\perp 0}^2}{2B_0}, \end{aligned} \tag{2}$$

further require that

$$V_{\|} = \pm V_0 \left[1 - \left|\frac{B}{B_0}\right|\left(1 - \zeta_0^2\right) + \frac{2e}{mV_0^2}(\phi - \phi_0)\right]^{1/2}, \tag{3}$$

where ϕ is the electrostatic potential. The quantity $\zeta_0 = V_{\|0}/V_0$ is the cosine of the initial guiding center velocity relative to the toroidal magnetic field direction.

As an aside, Eq. (3) determines the conditions (on W_0 and ζ_0) necessary for banana trapping (i.e., for $V_{\|}$ to vanish),

$$W_0 \le W_0^{\max} = \frac{e(\phi - \phi_0)}{\left[1 - \frac{B}{B_0}\left(1 - \zeta_0^2\right)\right]}. \tag{4}$$

Using Eq. (3) in Eq. (1) and squaring leads to a quadratic equation in the initial ion velocity $V_0 = \sqrt{V_{\|0}^2 + V_{\perp 0}^2}$,

$$\begin{aligned} &V_0^2\left[\left(\left|\frac{B}{B_0}\right|\frac{f_{\varphi 0}}{f_{\varphi}}\zeta_0\right)^2 - 1 + \left(1 - \zeta_0^2\right)\left|\frac{B}{B_0}\right|\right] \\ &+ V_0\left[\frac{2e(\psi_o - \psi)}{Rmf_{\varphi}}\left(\left|\frac{B}{B_0}\right|\frac{f_{\varphi 0}}{f_{\varphi}}\zeta_0\right)\right] \\ &+ \left[\left(\frac{e(\psi_0 - \psi)}{Rmf_{\varphi}}\right)^2 - \frac{2e(\phi_0 - \phi)}{m}\right] = 0. \end{aligned} \tag{5}$$

Note that Eq. (5) is quite general with respect to flux surface geometry representation of R, B, and the flux surfaces ψ. By specifying an initial "0" location for an ion with initial direction cosine ζ_0, and specifying a final location on flux surface ψ, Eq. (5) can be solved for the minimum initial ion speed V_0 that is required in order for the ion orbit to reach the final location (that the solution of Eq. (5) defines the minimum velocity will be shown below for the circular flux surface model). Thus, Eq. (5) can be solved for the minimum ion energy necessary for an ion located on an internal flux surface to cross the last closed flux surface at a given location or to strike the chamber wall at a given location, etc.

In order to illustrate the use of Eq. (5), we now specialize to the circular flux surface geometry described by

$$\begin{aligned} &[R(r,\theta) = \overline{R}h(r,\theta),\ B_{\theta,\varphi}(r,\theta) = \overline{B}_{\theta,\varphi}/h(r,\theta), \\ &\quad h(r,\theta) = (1 + (r/\overline{R})\cos\theta)]. \end{aligned} \tag{6}$$

Further specifying a uniform current density, Ampere's law and $B_{\theta} = \nabla \times A_{\varphi}$ can be used to write the flux surfaces as

$$\psi = RA_{\varphi} = \frac{1}{2}\left(\frac{\mu_0 I}{2\pi a^2}\right)\overline{R}r^2, \tag{7}$$

where I is the plasma current and a is the plasma minor radius.

We use as model parameters the parameters from a specific DIII-D plasma $(\overline{R} = 1.75\,m, a = 0.84\,m, I = 2.0\,MA, B_{\varphi} = -2.0T)$, with the plasma current flowing in the counter-clockwise direction looking down on the tokamak and the toroidal magnetic field in the opposite clockwise direction. The curvature and grad-B drifts are vertically downward in this model. The minor radius "a" of the effective circular model was chosen to preserve the area of the last closed flux surface of the elongated plasma. In this plasma model, the potential difference between some internal flux surface and the outermost last closed flux surface can be obtained from measurements of the local radial electric field by integrating to obtain the electrostatic potential, as in Fig. 1 for the specific DIII-D 123301 shot being used as a model problem. The model problem shot 123301 was a resonant magnetic perturbation (RMP) shot, and the electric field for an otherwise similar H-mode shot without RMP is also shown.

As an example, we examine the loss of ions flowing in the counter-current direction parallel to the toroidal magnetic field, for which $0 \le \zeta_0 \le 1$. The minimum energy calculated from Eq. (5) for which counter-current ions initially located at various points on the internal flux surface at r = 0.80 m ($\rho = 0.952$) can escape across any point on the last closed flux surface at a = 0.84 m is shown, for various directional cosines, in Fig. 2.

The energy (or velocity) calculated from Eq. (5) satisfies both Eqs. (1) and (3), which were combined to obtain Eq. (5). In the circular flux surface model, using Eq. (7) in Eq. (1) leads to an expression for the excursion from the "0" flux surface,

$$\left(r^2 - r_0^2\right) = \frac{4\pi a^2 m}{e\mu_0 I}\left[h(r,\theta)V_0\zeta_0 - h(r_0,\theta_0)V_{\|}(r,\theta)\right]. \tag{8}$$

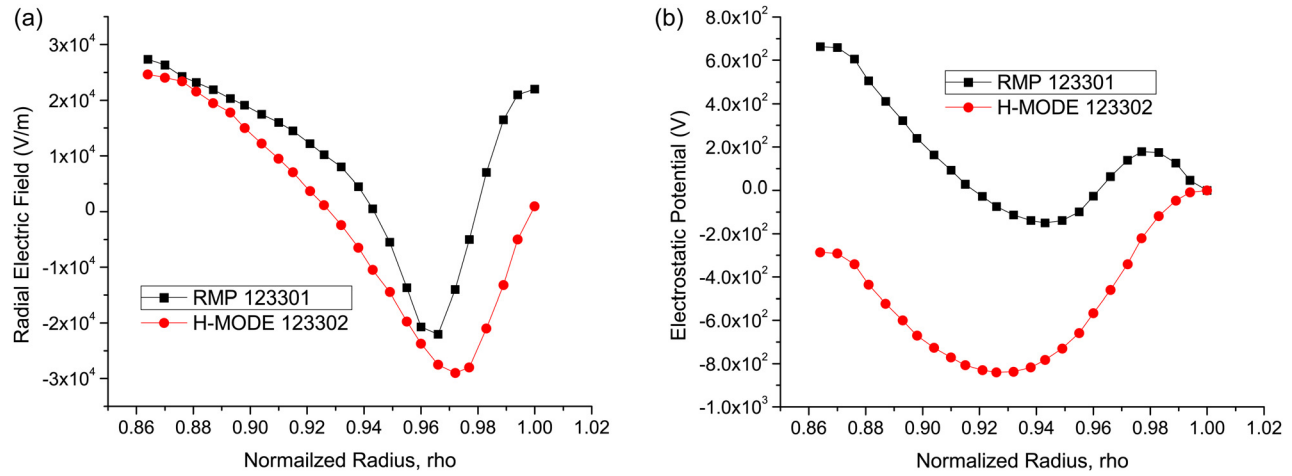

FIG. 1. (Color online) (a) Experimental electric fields and (b) electrostatic potentials from Fig. 1(a).

The value of V_0 obtained from Eq. (5) also satisfies Eq. (8), so any larger value of V_0 would correspond to a larger displacement to a flux surface with $r' > r$, requiring that the ion also cross flux surface r. Thus, the value of V_0 obtained from solution of Eq. (5) is the minimum value for which the ion would cross the flux surface at $r > r_0$.

The minimum initial energy required for an ion with direction cosine ζ_0 located at poloidal position θ_0 on flux surface "0" to be able to cross the last closed flux surface "D" (at $r_D = a$) at poloidal location θ_D can be calculated from Eq. (5). The smallest such energy for all values of θ_D is the minimum energy required for an ion with direction cosine ζ_0 located at poloidal position θ_0 on flux surface "0" to be able to cross the last closed flux surface "D" (at $r_D = a$). (We adopt the notation $\theta = 0$ at the outboard midplane, $\theta = \pi/2$ at the top, $\theta = \pi$ at the inboard midplane, and $\theta = 3\pi/2$ at the bottom of the plasma.) This minimum energy is $1/2mV_{0\min}^2$, where $V_{0\min}$ is the minimum energy calculated from Eq. (5) for which an ion located initially at a poloidal location θ_0 on the flux surface at $r_0 = 0.725$ m could cross the outer flux surface at $r_D = a = 0.84\,m, \rho = 1.0$ at any angular location. This minimum energy is the quantity plotted as a function of the location θ_0 of the ion on the interior flux surface at $r_0 = 0.72\,m, \rho_0 = 0.864$.

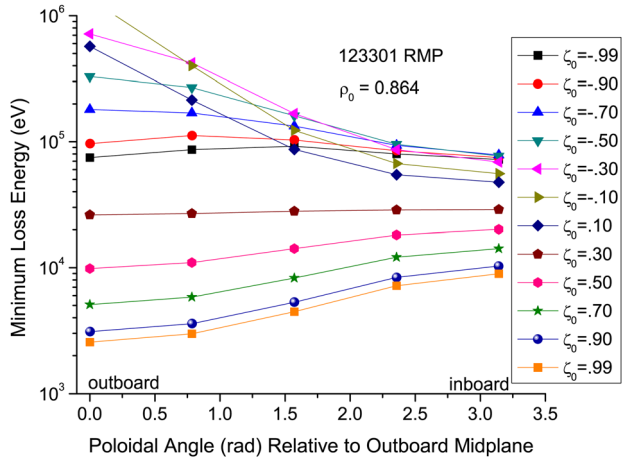

FIG. 2. (Color online) Minimum energy for standard ion orbit loss from $\rho = 0.864$ flux surface.

Since all ions with energies above the minimum value shown in Fig. 2, for each value of the direction cosine, have been lost by ion orbit loss when the ion flux crosses the flux surface at $\rho = 0.864$, Fig. 2 also depicts the ion energy-angle distribution in the plasma at this flux surface. The distribution of counter-current moving ions over $0 \le \zeta_0 \le 1$ is assumed to be a Maxwellian truncated above the energy indicated in Fig. 2. The distribution over $-1 \le \zeta_0 \le 0$ is to be Maxwellian in energy.

The measured ion temperature distribution for the DIII-D shot from which the model problem parameters are taken is shown in Fig. 3. It is clear from visual comparison of Figs. 2 and 3 that many of the Ctr-current directed ions with $0 \le \zeta_0 \le 1$ would be lost in the plasma edge.

The results shown in Fig. 3 can be used to calculate a loss region in velocity space, which, together with knowledge of the particle distribution function in velocity space, allows a particle loss rate to be calculated. (For the moment, we neglect scattering effects.) Designating the angle made by the initial ion velocity with the toroidal magnetic field ϑ (i.e., $\zeta_0 = \cos\vartheta$), the differential volume element in spherical velocity space is $(Vd\vartheta)(2\pi V\sin\vartheta)dV = -2\pi V^2 dV d\zeta_0$. The number of ions lost within $d\vartheta$ about a given ϑ is the number within $d\vartheta$ with $V \ge V_{\min}(\zeta_0)$. If the ions are distributed in velocity as $f(V)$, then the number of ions within $d\vartheta$ about a given ϑ which are lost is

$$dN_{loss}(\vartheta) = 2\pi\sin\vartheta\int_{V_{\min}(\vartheta)}^{\infty} V^2 f(V)dVd\vartheta = -2\pi\int_{V_{\min}(\zeta_0)}^{\infty} V^2 f(V)dVd\zeta_0. \quad (8)$$

At each poloidal location θ_0, the minimum energy for which an ion with direction cosine $1 \ge \zeta_0 \ge 0$ can escape across the last closed flux surface can be determined from Eq. (5), e.g., as shown in Fig. 2. The total loss rate from the flux surface of ions that escape across the last closed flux surface is obtained by integrating Eq. (8) over $1 \ge \zeta_0 \ge -1$,

$$N_{loss} = 2\pi\int_{-1}^{1}\left[\int_{V_{0\min}(\zeta_0)}^{\infty} V_0^2 f(V_0)dV_0\right]d\zeta_0. \quad (9)$$

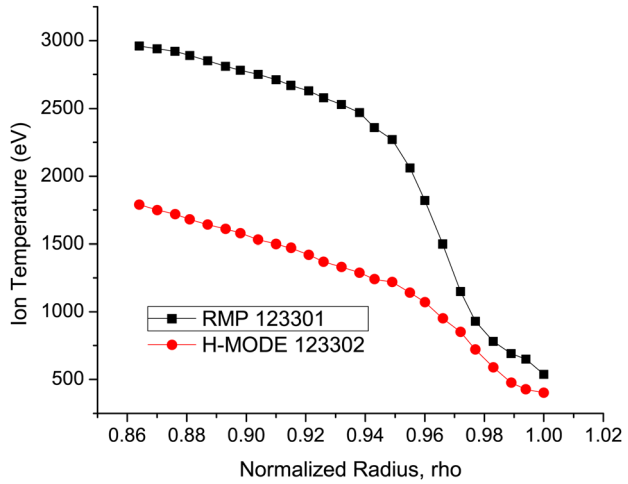

FIG. 3. (Color online) Measured ion temperature distributions for DIII-D discharges.

The total number of ions on the flux surface before any loss is

$$N_{tot} = 2\pi \int_{-1}^{1} d\zeta_0 \int_0^{\infty} V_0^2 f(V_0) dV_0, \tag{10}$$

leading to a definition of the ion loss fraction

$$F_{orb} \equiv \frac{N_{loss}}{N_{tot}} = \frac{\int_{-1}^{1} \left[\int_{V_{0\min(\zeta_0)}}^{\infty} V_0^2 f(V_0) dV_0 \right] d\zeta_0}{2 \int_0^{\infty} V_0^2 f(V_0) dV_0}. \tag{11}$$

When it is justifiable to use the Maxwellian velocity distribution, then

$$F_{orb} = \frac{\int_{-1}^{1} \int_{\varepsilon_{\min(\zeta_0)}}^{\infty} \varepsilon^{1/2} e^{-\varepsilon} d\varepsilon d\zeta_0}{2 \int_0^{\infty} \varepsilon^{1/2} e^{-\varepsilon} d\varepsilon} = \frac{\int_{-1}^{1} \Gamma\left(3/2, \varepsilon_{\min(\zeta_0)}\right) d\zeta_0}{2\Gamma(3/2)}, \tag{12}$$

where $\varepsilon_{\min}(\zeta_0) = mV_{0\min}^2(\zeta_0)/2kT$ is the reduced energy corresponding to the minimum velocity for which ion orbit loss is possible (e.g., as shown in Fig. 2).

A similar derivation leads to an expression for the energy loss fraction,

$$E_{orb} = \frac{\int_{-1}^{1} \left[\int_{V_{0min}(\zeta_0)}^{\infty} \left(\frac{1}{2} m V_0^2\right) V_0^2 f(V_0) dV_0 \right] d\zeta_0}{\int_{-1}^{1} \left[\int_0^{\infty} \left(\frac{1}{2} m V_0^2\right) V_0^2 f(V_0) dV_0 \right] d\zeta_0}$$
$$= \frac{\int_{-1}^{1} \int_{\varepsilon_{\min(\zeta_0)}}^{\infty} \varepsilon^{3/2} e^{-\varepsilon} d\varepsilon d\zeta_0}{2 \int_0^{\infty} \varepsilon^{3/2} e^{-\varepsilon} d\varepsilon} = \frac{\int_{-1}^{1} \Gamma\left(5/2, \varepsilon_{\min(\zeta_0)}\right) d\zeta_0}{2\Gamma(5/2)}, \tag{13}$$

where $\Gamma(n)$ is the gamma function of order n, and $\Gamma(n, \varepsilon_{\min})$ is the incomplete gamma function of order n.

These expressions were evaluated for the RMP discharge 123301 and for the otherwise similar "sister" H-mode shot 123302 (without RMP) at several values of the radius in the plasma edge, using the measured ion temperature profiles in Fig. 3. (Note that since only ions with $0 \le \zeta_0 \le 1$ were considered, the limits in the loss integrals in the numerators of Eqs. (12) and (13) were limited to this range.) The quantities $\Gamma(3/2, \varepsilon_{\min}(\zeta_0))/2\Gamma(3/2)$ and $\Gamma(5/2, \varepsilon_{\min}(\zeta_0))/2\Gamma(5/2)$, which are the fraction of ions and ion energy, respectively, that are lost across the separatrix by ion orbit loss from the flux surface at $\rho = 0.864$, are plotted in Fig. 4 as a function of the direction cosine of the ion motion relative to the positive toroidal direction defined by the current direction. The required energy of Ctr-current ions to reach the separatrix is in the thermal range (comparable to the local ion temperature), so a significant number of Ctr-current ions are able to escape, whereas the required energy of Co-current ions to reach the separatrix is very large and very few of them escape across the separatrix. (Different "co/ctr terminology are in common use. In this paper, "co" refers to ions moving in the direction of the plasma current, which is opposite to the direction of the toroidal field in these shots.)

Integrating the loss fractions of Fig. 4 over the direction cosine distribution (assumed uniform) yields the cumulative particle and energy loss fractions of Eqs. (12) and (13). These are plotted as a function of radial location in Fig. 5, for both the RMP and, otherwise similar, H-Mode shots. The magnitude of these standard ion orbit effects is much more significant in the RMP discharge than in the "sister" H-Mode discharge. In fact, the effect of the RMP to produce the change in the H-mode electric field shown in Fig. 1, which produces enhanced ion orbit loss, may well be one mechanism by means of which the RMP produces the density reduction below the Edge-Localized-Modes (ELM) threshold.

Figure 5 represents a cumulative loss fraction out to radius r. In other words, the loss region in velocity space at radius r_1 also includes the lost regions for all smaller radii $r < r_1$. This loss region expands with radius as the radius approaches the last closed flux surface, and the minimum speed for which a particle with $0 \le \zeta_0 \le 1$ can be lost decreases with radius.

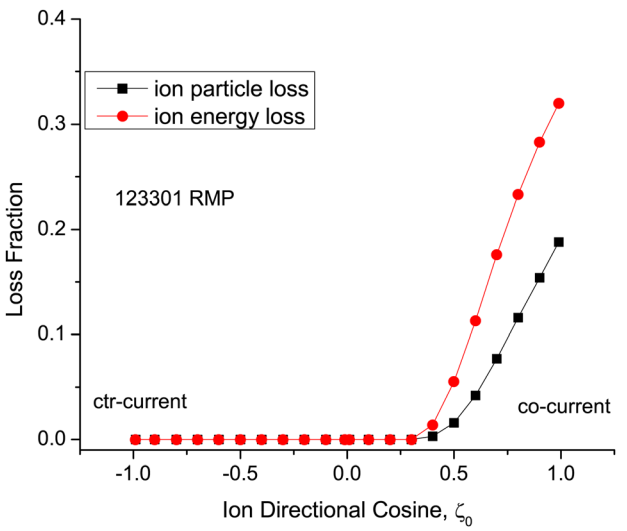

FIG. 4. (Color online) Loss fractions as a function of ion direction from flux surface at $\rho = 0.864$. (The ion direction cosine is with respect to the magnetic field direction.)

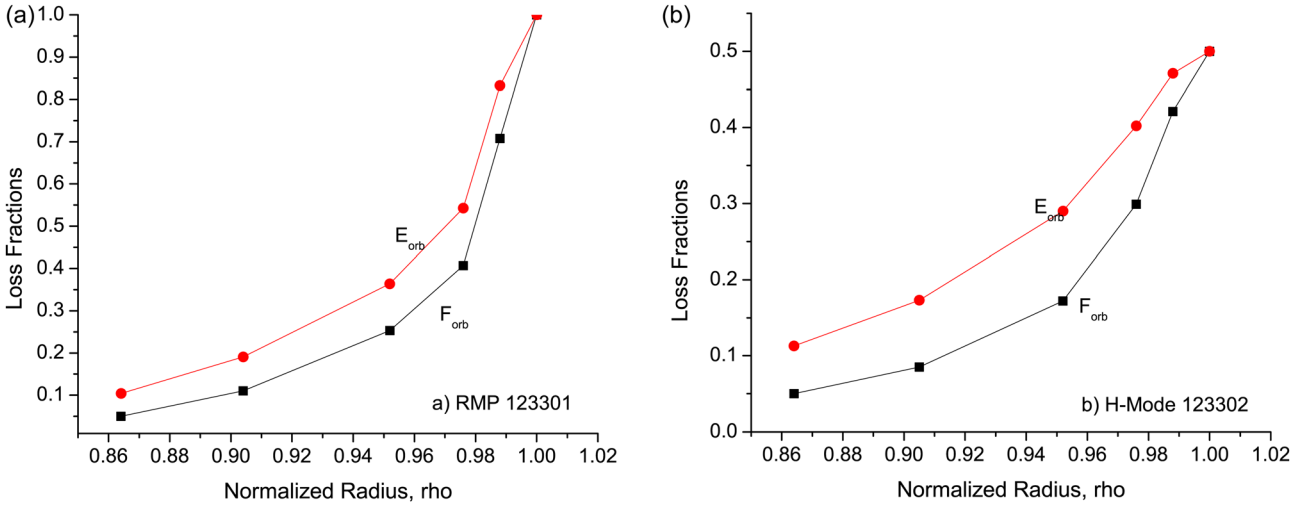

FIG. 5. (Color online) Ion particle (lower curves) and energy (upper curves) cumulative loss fractions for DIII-D (a) RMP and (b) otherwise similar H-Mode discharges.

III. MODELING OF ION ORBIT X-LOSS

The standard ion orbit loss treated in Sec. II involved particles following the spiraling field lines and drifting across them until their orbit intersected the separatrix.

A distinctly different ion orbit loss mechanism is introduced by the presence of a divertor X-point, which is a null point for the poloidal magnetic field. In a region about the X-point the poloidal field is very small, $B_\theta \ll \varepsilon B_\phi$, and the field lines are almost purely toroidal and do not spiral about the tokamak to provide the usual neoclassical cancellation of drift effects. On the other hand, ions quite rapidly move poloidally over the remainder of the flux surface by following along spiraling field lines, as they approach the X-point their poloidal motion is provided only by the slower poloidal $E_r \times B_\phi$ drift due to the radial electric field. This poloidal drift will move the ions poloidally into and across the null-B_θ region near the X-point until they again enter a region in which $B_\theta \approx \varepsilon B_\phi$ once again and they can move rapidly poloidally over the flux surface by the spiraling motion of the field lines.

However, while the ions are slowly drifting poloidally across the null-B_θ region near the X-point, they are also drifting vertically due to curvature and grad-B drifts. In the configuration considered in this paper, with the toroidal field in the clockwise direction and the plasma current in the counter-clockwise direction, looking down on the tokomak, and with a lower single-null divertor, this vertical drift is downward towards the divertor. If the time required for the ion to grad-B drift downward across the separatrix is less than the time required for the ion to $E_r \times B_\phi$ drift across the $B_\theta \ll \varepsilon B_\phi$ region near the X-point, the ion will be lost across the separatrix. Even if the ion is not lost across the separatrix, it will be displaced radially while it is traversing the null-B_θ region. This is the essential physics of the X-loss and X-transport mechanism discussed by Chang, *et al.*[18–23]

We represent the geometry of the X-loss region by postulating a flux surface geometry defined by concentric flux surfaces described by a radius that is poloidally dependent, $r(\theta)$. In particular, the X-point is located on the separatrix flux surface at the poloidal angle θ_x so that $r_x = r_{sep}(\theta_x)$. We will consider lower single null divertors with $\theta_x = 3\pi/2$, but the formalism that will be developed can readily be extended to other divertor locations and more general flux surface geometry.

The poloidal magnetic field vanishes at the X-point, $B_\theta = 0$, and slowly increases to $B_\theta \approx \varepsilon B_\phi$ over a poloidal arc distance $r_{sep}(\theta_x)(\Delta\theta_x/2)$ on either side of $\theta = \theta_x$; i.e., $\left(1/r_{sep}(\theta_x)\right)(\partial B_\theta/\partial\theta) \times r_{sep}(\theta_x)(\Delta\theta_x/2) \approx \varepsilon B_\varphi$. The poloidal field also increases away from the X-point in the radial direction to $B_\theta \approx \varepsilon B_\phi$ over a distance Δr_x, i.e., $(\partial B_\theta/\partial r) \times \Delta r_x \approx \varepsilon B_\varphi$. The solenoidal law $0 = \nabla \bullet \mathbf{B}_\theta \approx (\partial B_\theta/\partial r) + (1/r)(\partial B_\theta/\partial r)$ relates the radial and poloidal variations of B_θ in the vicinity of the X-point. Combining these results leads to $\left(\Delta r_x/r_{sep}(\theta_x)\Delta\theta_x\right) \approx 1/2$. Since the X-loss mechanism is a competition between curvature and grad-B drifting a distance Δr_x before E×B drifting a distance $r_{sep}(\theta_x)\Delta\theta_x$, this result indicates that the calculation can be performed either in the actual flux surface geometry or in a transformed geometry (e.g., the effective circular flux surface geometry model described above) so long as the same radial transformation is used for r_{sep} and for Δr_x.

Thus, we may envision a tall wedge or trapezoidal shaped X-loss region extending radially inward (upward) from the X-point a distance Δr_x with width $r(\theta_x)\Delta\theta_x$ within which the motion of ions is determined by the radially outward (downward) curvature and grad-B drifts and by the poloidal $E_r \times B_\phi$ drift. While the ion is $E \times B$ drifting across the null-B_θ region it is also grad-B and curvature drifting radially outward (downward). The time required for an ion entering the plasma at radius r to gradB and curvature drift downward a distance Δr is

$$\tau_{\nabla B} = \frac{\Delta r}{V_{\nabla B,c}} = \frac{\Delta r}{\left(W_\perp + 2W_\parallel\right)/eRB} = \frac{eRB}{W\left(1+\zeta^2\right)}\Delta r, \quad (14)$$

where ζ is the cosine of ion direction with respect to the magnetic field and W denotes the ion energy. During this time the ion is also $E_r \times B_\phi$ drifting through a poloidal arc distance,

$$r(\theta_x)\Delta\theta = V_{E\times B}\tau_{\nabla B} = \frac{E_r(r)}{B_\phi}\frac{eRB}{W(1+\zeta^2)}\Delta r. \qquad (15)$$

Note that when the radial electric field changes sign (see Fig. 1), the directions of the poloidal drift and of the angular displacement both reverse.

We calculate the X-loss for an ion that $E_r \times B_\phi$ drifts into the X-loss region at a given radial location $r < r_{sep}$ by dividing the radius from the center of the plasma to the separatrix into increments Δr_n over each of which the plasma properties are approximated as constant, which allows the calculation of the change

$$\Delta\theta_n \simeq \frac{\Delta r_n}{r_n}\frac{eRE_{rn}}{W\left(1+\zeta^2\right)} \qquad (16)$$

in $\Delta\theta$ that will take place while the ion gradB drifts radially downward (outward) a distance Δr_n.

Thus, the determination of whether a particle that enters the X-loss region is in fact lost is just a matter of calculating $\Delta\theta_n$ successively for all regions between the radius of entry and the separatrix and summing. If the calculated sum becomes greater than $\Delta\theta_x$, or reverses sign, before the separatrix is reached, then the ion has drifted out of the X-loss region and does not escape across the separatrix. Note that if an ion poloidally $E_r \times B_\phi$ drifts into the X-loss region in one direction and then gradB drifts into a region in which the electric field changes sign, then the $E_r \times B_\phi$ drift direction also changes poloidal direction. A change in sign of the summed $\Delta\theta_n$ indicates that the ion has drifted out of the X-loss region on the same side on which it entered. Because $\Delta\theta_n$ is inversely proportional to the ion energy, the accessibility to X-loss is greater for higher energy ions. However, we find that there are some radii for entry into the X-loss region for which the ions can not be X-lost across the separatrix, except at extremely high energies, because a reversal in radial electric field sign causes them to drift out of the X-loss region before drifting across the separatrix.

The minimum ion energy at which ions can be X-lost with the electric field shown in Fig. 1 has been calculated for three plausible values of the angular extent of the X-loss region, $\Delta\theta_x = 0.1$, 0.15, and 0.2 radians. The corresponding X-loss regions extend in to $\rho = 0.955, 0.930, 0.904$, respectively. The minimum ion energies for X-loss are shown in Fig. 6. No X-loss ion energies were found for ions introduced near the radial locations at which the electric field reversed sign (calculations were carried out up to 20 keV ion energy).

In carrying out the calculations summarized in Fig. 6, we found that even when the successive summation of $\Delta\theta_n$ became greater than $\Delta\theta_x$ or changed sign, both indicating $E_r \times B_\phi$ drift out of the X-loss region back into the "tokamak" zone where $B_\theta \approx \varepsilon B_\phi$, it was sometimes at significantly increased radius. These both suggest an X-transport mechanism, due to this outward radial displacement of ions by gradB drift, and a way to calculate it. This task is beyond the scope of the present paper and involves a sizeable bookkeeping job, so we will defer it until a future paper.

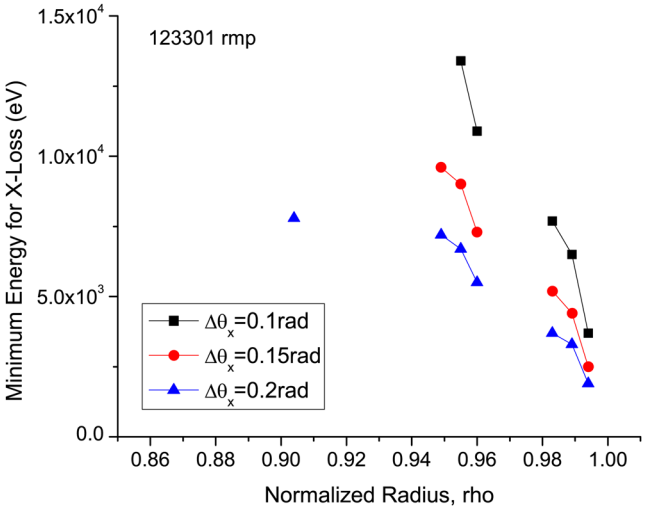

FIG. 6. (Color online) The minimum energy for X-loss of ions across the separatrix for the electric field distribution of DIII-D shot 123301 shown in Fig. 1(a).

The times required for ions to be swept poloidally around the flux surface by following along the field lines and to then $E_r \times B_\phi$ drift into the X-loss regions are short compared with the time required for the ions to flow radially outward (at about 1 m/s) across the flux surfaces. This implies that as the plasma flows radially outward across the flux surfaces the ion population is repeatedly swept through the X-loss region as the radial location increases, so that those ions with energies above the minimum energy for X-loss at that radial position are lost across the separatrix. Since there is little neutral beam injection into the edge and since the ionization of recycling neutrals creates low energy ions, there is no mechanism other than electron heating for the high energy plasma ions to be replaced once they are X-lost.

The fraction of ions entering the X-loss region at r which are X-lost through the separatrix is just the fraction of plasma ions $E_r \times B_\phi$ drifting into the X-loss region at any given radius that have energy greater than the minimum loss energy shown in Fig. 6. Defining $\varepsilon_{\min} \equiv W_{\min}(r)/T_i(r)$ and assuming a Maxwellian distribution yields an expression for the fraction of ions with $W \geq W_{\min}$,

$$F_x(r) = \frac{\int_{W_{min}(r:r')}^{\infty} f(W(r))dW}{\int_0^{\infty} f(W(r))dW} = \frac{\Gamma\left(\frac{3}{2}, \varepsilon_{\min}\right)}{\Gamma\left(\frac{3}{2}\right)}. \qquad (17)$$

Similarly, the fraction of the ion energy carried by the ions with $W \geq W_{\min}$ is

$$E_x(r) = \frac{\int_{W_{min}(r:r')}^{\infty} W(r)f(W(r))dW}{\int_0^{\infty} W(r)f(W(r))dW} = \frac{\Gamma\left(\frac{5}{2}, \varepsilon_{\min}\right)}{\Gamma\left(\frac{5}{2}\right)}. \qquad (18)$$

The X-loss factors of Eqs. (17) and (18), which define the fraction of ions and ion energy entering the null-B_θ region at a given radius that is lost by drifting down across the separatrix, are plotted in Fig. 7 for the RMP discharge. In flowing

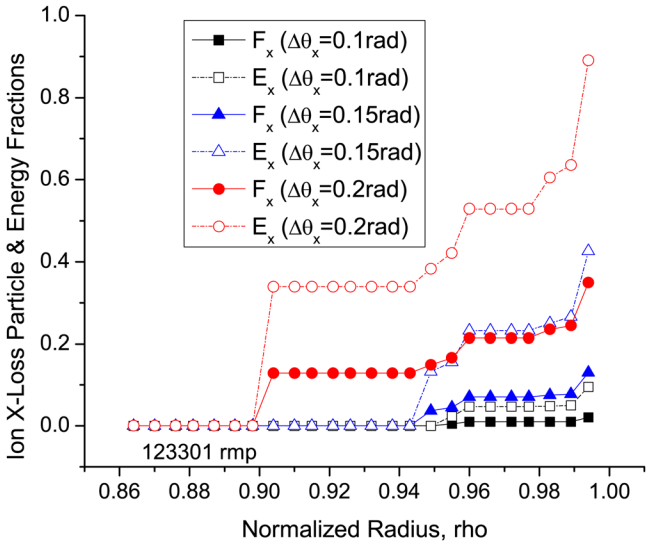

FIG. 7. (Color online) The X-Loss fractions for ion particle and energy for RMP shot 123301.

outward through radial regions in which there is not any X-loss (as indicated by the gaps in the curves in Fig. 6)), the plasma is not loosing any energy through the X-loss process, so it is assumed that cumulative X-loss of ions and ion energy remains unchanged.

IV. INCLUSION OF PARTICLE AND ENERGY ION ORBIT AND X-LOSS IN FLUID CALCULATIONS

Neglecting for the moment that scattering within the edge pedestal could repopulate the loss region, we will take standard ion orbit loss and X-loss into account in fluid calculations of the plasma edge by reducing the particle and energy fluxes calculated by the fluid codes by the appropriate loss functions; i.e., we will define the effective radial particle and energy fluxes,

$$\widehat{\Gamma}_i(r) = \Gamma_i(r)[1 - F_{orb}(r)], \quad \widehat{Q}_i(r) = Q_i(r)[1 - E_{orb}(r)], \tag{19a}$$

$$\widehat{\Gamma}_i(r) = \Gamma_i(r)[1 - F_{orb}(r)][1 - F_x(r)],$$
$$\widehat{Q}_i(r) = Q_i(r)[1 - E_{orb}(r)][1 - E_x(r)], \tag{19b}$$

corrected to take into account ion orbit losses (Eq. (19a)) or to take into account both ion orbit loss and X-loss (Eq. (19b)).

The radial ion flux can be calculated from the usual fluid continuity equation, taking into account ion sources in the plasma edge,

$$\frac{\partial \Gamma_i}{\partial r} = -\frac{\partial n_i}{\partial t} + n_e n_o \langle \sigma v \rangle_{ion} + S_{nb}. \tag{20}$$

The second term on the right represents the electron ionization of recycling neutral atoms of the main plasma species and the third term represents the source of plasma ions due to neutral beam injection.

The radial ion energy flux can be calculated from the fluid ion energy balance equation in the plasma edge, taking into account heating and cooling of the ions in the edge,

$$\frac{\partial Q_i}{\partial r} = -\frac{\partial}{\partial t}\left(\frac{3}{2} n_i T_i\right) + q_{nbi} - q_{ie} - n_e n_o^c \langle \sigma v \rangle_{cx} \frac{3}{2}(T_i - T_o^c). \tag{21}$$

Here, q_{nb} is the neutral beam (or other external) heating source rate, q_{ie} is the collisional heat exchange from ions to electrons, the subscript cx refers to charge-exchange plus elastic scattering, and the superscript c denotes the *cold* (i.e., not previously collided in the plasma edge) neutral atom species that have penetrated into the pedestal.

From an interpretive perspective, ion orbit loss does not change the magnitude of the ion flux or the ion energy flux that are calculated by solving Eqs. (20) and (21), but it does change how these fluxes are understood to be distributed among conduction, convection, and free-streaming. In the presence of ion orbit loss, the total ion heat flux is a sum of conductive, convective, standard ion orbit loss and X-loss components,

$$\begin{aligned} Q_i &= Q_i^{cond} + Q_i^{conv} + Q_i^{orb} + Q_i^x \\ &\equiv -n_i \chi_i \partial T_i / \partial r + 3/2 \Gamma_i T_i + E_{orb} Q_i + E_x Q_i. \end{aligned} \tag{22}$$

As an illustrative example of the importance of ion orbit loss and X-loss, this relation can be used, together with the total heat and particle fluxes calculated as described above, to interpret the experimental heat diffusivity from the temperature measurements given in Fig. 3 and similar measurements of the ion density profile,

$$\chi_i^{\exp} = \frac{\left(-\frac{1}{T_i}\frac{\partial T_i}{\partial r}\right)_{\exp}^{-1}}{n_i^{\exp} T_i^{\exp}} \times \left[Q_i(1-E_{orb})(1-E_x) - \frac{3}{2} T_i^{\exp} \Gamma_i (1-F_{orb})(1-F_x)\right]. \tag{23}$$

The reduction in the convective energy flux due to ions that become free-streaming or that are X-loss is also taken into account in this expression.

The total ion particle and heat fluxes obtained by solving Eqs. (20) and (21) for the model problem parameters, using the measured temperature and density distributions, is shown by the solid square symbols in Figs. 8 and 9. Taking into account the ion orbit loss, the ion particle and total (conductive plus convective) heat flux are then constructed (the latter according to Eqs. (19a)), using the standard ion orbit loss fractions given in Fig. 5(a), and the results are plotted as the solid circle symbols in Figs. 8 and 9. Finally, the standard ion orbit loss and the X-loss are both taken into account by using Eq. (19b), and the results are plotted with the solid triangle symbols in Figs. 8 and 9. The X-loss calculation used an average value of $\zeta = 0.5$ and $\Delta\theta_x = 0.15$ radians. There is a significant reduction in the conductive and convective heat fluxes and in the ion particle flux, relative to the values calculated from the particle and energy balance equations, due to standard ion orbit loss, and a somewhat lesser reduction due to X-loss.

In order to characterize the importance of the ion orbit loss effects on ion particle and heat fluxes shown in Figs. 8 and 9, we used Eq. (23) to interpret the ion thermal

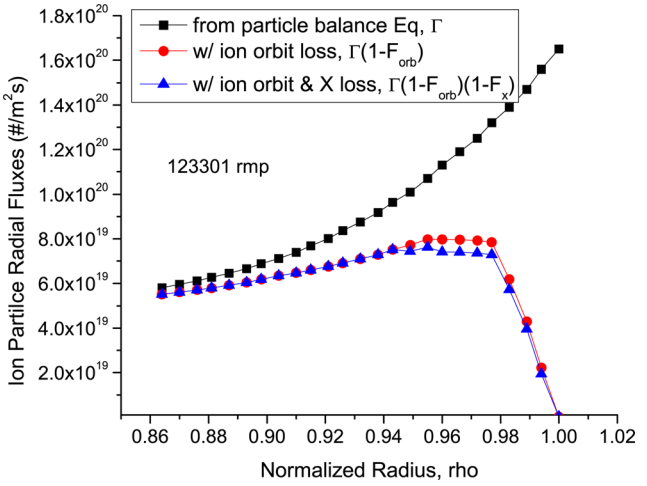

FIG. 8. (Color online) Convective/diffusive ion particle fluxes with and without ion orbit loss and X-loss.

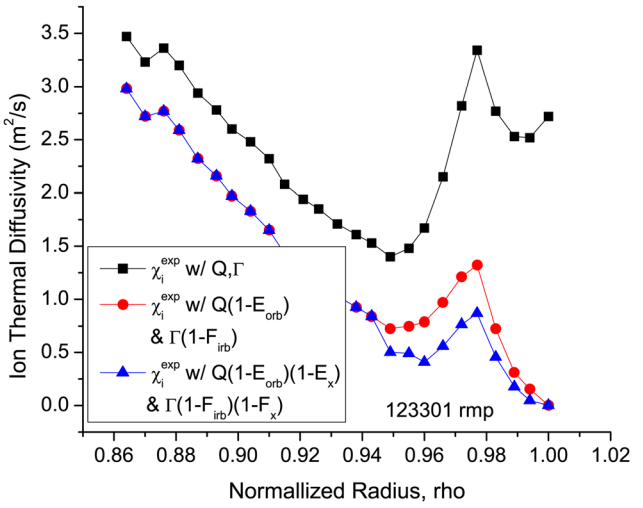

FIG. 10. (Color online) Ion thermal diffusivities interpreted from the measured ion temperature profile given in Fig. 3 using Eq. (23) and the heat fluxes of Fig. 5 with and without ion orbit loss.

diffusivity from the measured ion temperature distribution of Fig. 3, first without either standard ion orbit loss or X-loss (solid square symbols), then with ion orbit loss corrections (solid circle symbols), and finally with both ion orbit loss and X-loss corrections (solid triangle symbols). The results given in Fig. 10 indicate a significant difference in the value of the thermal diffusivity interpreted from experimental data when standard ion orbit loss effects are taken into account, and a somewhat less additional difference when X-loss effects are taken into account. The specifics will, of course, differ for different shots, but this result provides an estimate of the magnitude of the ion orbit loss effects.

The dip just inside the separatrix in inferred experimental thermal diffusivity shown in Fig. 10 is a new result not seen in our previous interpretation[38] of shot 123301 and arising from a refined analysis of the experimental data (by T. E. Evans). This result is suggestive of a reduction in the ion thermal diffusivity just inside the separatrix due to the RMP, which would be consistent with the higher ion temperature in the RMP shot than in the otherwise similar H-mode shot shown in Fig. 3. It is planned to make a detailed comparison

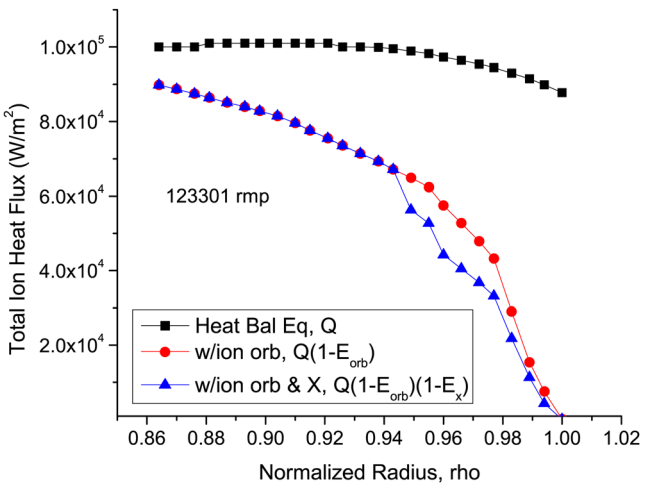

FIG. 9. (Color online) Total ion heat flux calculated from ion heat balance equation and corrected for ion orbit and X-loss.

of this and other differences between these two shots that may be associated with differences in ion orbit loss in a future paper.

There is a further effect of ion orbit and X-loss on the fluid model results. Since both mechanisms result in a loss of all ions above a certain energy W_{min}, which decreases with increasing radius, the ion distribution function is in the first approximation a truncated Maxwellian with the truncation energy decreasing with radius. Such a distribution could be used to iteratively recompute the fluid transport coefficients.

V. SCATTERING

The effects of scattering have been neglected in the derivation up to this point. There are two potential effects of scattering on standard ion orbit loss: (i) some of the ion orbit loss particles identified in Sec. II could be scattered out of the loss orbit before crossing the last closed flux surface, which would reduce the loss fraction and (ii) particles with initial directions that would not be lost could be scattered to repopulate loss regions and enhance the loss fraction. If the time required for the loss orbit to be traversed, $\tau_{loss} = \ell_{orbit}/V_0\zeta_0 \approx qR/V_0\zeta_0$, is short compared to the 90 scattering time ν_{iz}^{-1} of deuterium ions scattering from carbon impurity ions, scattering can be ignored. This requirement can be written as

$$\frac{t_{loss}}{\nu_{iz}^{-1}} = \nu_{iz}\frac{qR}{V_0\zeta_0} = \frac{\nu_{iz}qR}{V_{thi}}\frac{V_{thi}}{V_0\zeta_0} \equiv \frac{\nu_{iz}^*}{\sqrt{\varepsilon}\zeta_0} \equiv \nu_{iz}^{**} << 1, \quad (24)$$

where $\varepsilon = mV_0^2/2kT$. The quantity ν_{iz}^{**} has been evaluated using the values of ν_{iz}^* for these discharges given in Fig. 11, and the minimum value of the corresponding ε found by dividing the minimum energies for orbit loss such as shown in Fig. 2 by the local ion temperature shown in Fig. 3. Except for very small values of ζ_0, the component of motion along the field line, $\nu_{iz}^{**} \ll 1$, justifying neglect of scattering. (Note that $\nu_{ii} = (n_i/z^2n_z)\nu_{iz} \simeq \nu_{iz}$.)

Rewriting Eq. (24) suggests how to correct the standard ion orbit loss calculations for the effects of scattering by

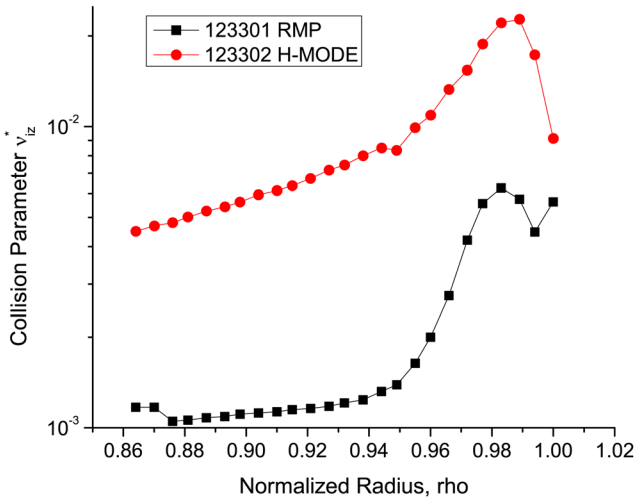

FIG. 11. (Color online) The collisionality parameter $\nu^*_{iz} = qR\nu_{iz}/V_{thi}$.

defining a minimum ion normalized energy that will result in the collisionality parameter ν^{**}_{iz} being less than the maximum value for which the probability of a 90 scattering collision taking place before the particle escapes across the last closed flux surface is less than some maximum value (e.g., $(\nu^{**}_{iz})_{\max} = 0.1$),

$$\sqrt{\varepsilon^{scat}_{\min}} \equiv \frac{\nu^*_{iz}}{(\nu^{**}_{iz})_{\max}\zeta_0}. \tag{25}$$

If the corresponding minimum energy $E^{scat}_{\min} \equiv 1/2mV^2_{0\min} = \varepsilon^{scat}_{\min}kT_i$ is greater than the minimum energy for orbit loss given in Fig. 2, then $E^{scat}_{\min}$ would replace the minimum energy for orbit loss in the determination of the loss fractions described in Sec. II (i.e., the incomplete gamma functions would be evaluated using $\varepsilon^{scat}_{\min}$ instead of the $\varepsilon_{\min}$ for orbit loss determined from Fig. 2).

VI. DISCUSSION AND CONCLUSIONS

A calculation of ion orbit loss from interior flux surfaces was carried out for model problems representative of two DIII-D discharges. Both the "standard" ion orbit loss, in which ions follow trapped or passing drift orbits that cross the separatrix, and "X-loss," in which ions become poloidally trapped in the narrow null-B_θ region extending into the plasma from the X-point where gradB/curvature drift carries them outward across the separatrix were considered. Although these two loss mechanisms have been treated as independent, strictly speaking they are not (e.g., Ref. 39), because ions lost by one mechanism are not available to be lost by the other mechanism. Since all the ions above a certain minimum energy are lost for each loss mechanism, it would be possible to take this into account using the formalism of this paper. For example, if the minimum loss energy $W_{\min 1} = W_{\min 2}$, then the loss by mechanism 2 (e.g., ion orbit loss) could be reduced by the loss already included in mechanism 1 (e.g., X-loss), or vice-versa. This is not an issue for the model problem discharges discussed in the paper in which the ion orbit loss was much larger than the X-loss.

Another assumption made in the application of the ion orbit loss formalism was that an ion was lost if it crossed the separatrix. Some ions on such orbits will re-enter the confined plasma. It is possible to represent the chamber wall, rather than the separatrix, as the lost surface using the formalism presented in this paper, and it is possible in principle to calculate the probability that an ion will be lost by charge exchange while traversing the scrape-off layer outside the separatrix.

Computational models for treating these ion orbit loss mechanisms in interpretive fluid calculations of the edge plasma were presented and employed to evaluate the magnitude of ion orbit loss effects in DIII-D. It is concluded that such effects are significant in DIII-D (and probably in other experiments) and that their neglect in present interpretive analyses results in a significant overestimation of the experimental ion thermal diffusivity in the edge pedestal. Ion orbit loss should be taken into account in both interpretive and predictive calculations of present and future experiments.

ACKNOWLEDGMENTS

The author would like to acknowledge useful information on the poloidal magnetic field configuration in DIII-D obtained in communications with Todd Evans and Mike Shaffer and to acknowledge the efforts of the DIII-D Team in making the measurements used in this paper. This work was supported by the U. S. Department of Energy under Grant No. FE-FG01-ER54538 with the Georgia Tech Research Corporation.

[1]A. E. Hubbard, Plasma Phys. Controlled Fusion **42**, A15 (2000).
[2]C. F. Maggi, Nucl. Fusion **50**, 066001 (2010).
[3]R. J. Groebner, K. H. Burrell, and R. P. Seraydarian, Phys. Rev. Lett. **64**, 3015 (1990).
[4]W. M. Stacey and R. J. Groebner, Phys. Plasmas **17**, 112512 (2010).
[5]W. M. Stacey and R. J. Groebner, Nucl. Fusion **51**, 063024 (2011).
[6]W. M. Stacey and T. E. Evans, Nucl. Fusion **51**, 013007 (2011).
[7]H. Biglari, P. H. Diamond, and P.W. Terry, Phys. Fluids B **2**, 1 (1989).
[8]K. H. Burrell, Phys. Plasmas **4**, 1499 (1997).
[9]P.W. Terry, Rev. Mod. Phys. **72**, 109 (2000).
[10]F. L. Hinton and M. Chu, Nucl. Fusion **25**, 345 (1985).
[11]K. Miyamoto, Nucl. Fusion **36**, 927 (1996).
[12]K. C. Shaing and E. C. Crume, Phys. Rev. Lett. **63**, 2369 (1989).
[13]K. C. Shaing, E. C. Crume, and W. A. Houlberg, Phys. Fluids B **2**, 1492 (1990).
[14]K. C. Shaing, Phys. Fluid B **4**, 171 (1992).
[15]K. C. Shaing, Phys. Plasmas **9**, 1 (2002).
[16]G. F. Matthews, G. Corrigan, S. K. Erents, W. Fundamenski, A. Kallenbach, T. Kurki-Suonio, S. Sipila and J. Spence, JET Report EFDA-JET-CP(02)01-02, 2002.
[17]J. S. DeGrassie, R. J. Groebner, K. H. Burrell, and W. M. Solomon, Nucl. Fusion **49**, 085020 (2009).
[18]C. S. Chang, S. Kue, and H. Weitzner, Phys. Plasmas **9**, 3884 (2002).
[19]C. S. Chang, S. Kue, and H. Weitzner, Phys. Plasma **11**, 2649 (2004).
[20]H. Weitzner and C. S. Chang, Phys. Plasmas **11**, 3060 (2004).
[21]C. S. Chang, Phys. Plasmas **11**, 5626, (2004).
[22]S. H. Hahn, S. Ku, and C. S. Chang, Phys. Plasmas **12**, 102501 (2005).
[23]C. S. Chang and S. Ku, Phys. Plasmas **15**, 062510 (2008).
[24]M. A. Mahdavi, R. Maingi, R. J. Groebner, A. W. Leonard, T. H. Osborne, and G. Porter, Phys. Plasmas **10**, 3984 (2003).
[25]R. J. Groebner, M. A. Mahdavi, A. W. Leonard, T. H. Osborne, N. S. Wolf, G. D. Porter, P. C. Stangeby, N. S. Brooks, R. J. Colchin, and L. W. Owen, Nucl. Fusion **44**, 204 (2004).
[26]P. B. Snyder, H. R. Wilson, J. R. Ferron, L. L. Lao, A. W. Leonard, T. H. Osborne, A. D. Turnbull, and X. Q. Xu, Nucl. Fusion **44**, 320 (2004).
[27]M. Kotschenreuther, W. Dorland, Q. P. Liu, G. W. Hammett, M. A. Beer, S. A. Smith, A. Bondeson, and S. C. Cowley, *Proceedings of the 16th*

Conference on Plasma Physics Controlled Fusion Research, Montreal, 1996 (IAEA, Vienna, 1997), Vol. 2, p.371.
[28]J. E. Kinsey, R. E. Waltz, and D. P. Schissel, *Proceedings of the 24th Conference on European Physical Society, Berchtesgarten* EPS, Geneva, 1997, Vol. 3, p.1081.
[29]J. D. Callen, R. J. Groebner, T. H. Osborne, J. M. Canick, L. W. Owen, A. Y. Pankin, T. Rafiq, T. D. Rognlien and W. M. Stacey, Nucl. Fusion **50**, 064004 (2010).
[30]H. E. St. John, T. S. Taylor, Y.-R Lin-Liu and A. D. Turnbull, *Proceedings of the 15th Conference on Plasma Phys .Control. Fusion, Seville, 1994* Vienna, IAEA, 1995, Vol. 3, p. 60.
[31]W. M. Stacey, Phys. Plasmas **5**, 1015 (1998); *ibid.* **8**, 3673 (2001); Nucl. Fusion **40**, 965 (2000).
[32]T. D. Rognlien and M. E. Rensink, Fusion Eng. Des. **60**, 497 (2002).
[33]R. Schneider, X. Bonnin, K. Borrass, D. P. Coster, H. Kastelewicz, D. Reiter, V. A. Rozhansky, and B. J. Braams, Contrib. Plasma Phys. **46**, 3 (2006).
[34]W. M. Stacey, Phys. Plasmas **15**, 052503 (2008).
[35]J. Luxon, Nucl. Fusion **42**, 614 (2002).
[36]A. Chankin and G. McCracken, Nucl. Fusion **33**, 1459 (1993).
[37]N. Azarenkov and Zh. Kononenko, J. Kharkiv Univ. **859**, 51 (2009).
[38]W. M. Stacey and T. E. Evans, Phys. Plasmas **13**, 112506 (2006).
[39]S. Ku, H. Baek and C. S. Chang, Phys. Plasmas **11**, 5626 (2004).